Porous Networks

DOI: 10.1002/anie.201101477

Two-Dimensional Molecular Porous Networks Formed by Trimesic Acid and 4,4′-Bis(4-pyridyl)biphenyl on Au(111) through Hierarchical Hydrogen Bonds: Structural Systematics and Control of Nanopore Size and Shape**

Hailin Liang, Wei Sun, Xin Jin, Heng Li, Jianlong Li, Xinquan Hu, Boon K. Teo,* and Kai Wu**

Two-dimensional (2D) molecular porous networks (MPNs) self-assembled on surfaces are of great interest due to their potential applications in nanoscience.[1–3] Conventionally, the assembled molecules are held together by non-covalent interactions,[4–10] among which the hydrogen bond (HB) is frequently adopted for structural controllability owing to its desirable bonding strength, selectivity, and directionality.[1] This strategy has been utilized in both uni-[6] and bimolecular[11–15] systems. Generally speaking, hydrogen bonds of similar bond strength are less versatile than hierarchical ones in tuning the assembled structures. In nature, hierarchical hydrogen-bond systems with disparate bonding capabilities and strengths are widely adopted by biosystems such as DNA and bioactive structures which consist of only limited building blocks. Researchers have utilized metal coordination[16,17] or hydrogen bonds[4,18] to form various porous networks on surfaces. Controls of the network pattern and the resulting pore size and shape can be achieved by tuning parameters[17,19–21] such as ligand chain lengths or molecular backbones,[19] surface coverage[20] and substrate temperature.[22] These strategies have been demonstrated for a number of uni-[16,20] or bimolecular systems.[18,23] For example, by adjusting the metal-to-ligand ratio and the annealing temperature, mononuclear, 1D-polymeric and 2D-reticulated metal–organic coordination networks can be obtained by vapor deposition of 1,4-benzenedicarboxylic acid molecules and iron atoms on a Cu(100) surface, giving rise to an interesting series of square, rectangular and rhombic pores.[16] Another excellent example demonstrating controls of the network pattern and pore morphology is the 2D mono- and bicomponent self-assembly of three closely related diaminotriazine-based molecular building blocks and a complementary perylenetetracarboxylic diimide on Au(111) surface. The interplay, and the hierarchy, of hydrogen bonding, metal-ligand coordination, and dipolar interactions, resulted in various MPNs. In one case, mixtures of square, rhombic, and hexagonal nanopores were obtained.[24] A third example illustrating the construction of tunable 2D binary molecular nanostructures on an inert surface is the co-deposition of copper hexadecafluorophthalocyanine with *p*-sexiphenyl, pentacene, or diindenoperylene on graphite. By varying the binary molecular ratio and the molecular geometry, various molecular networks with tunable intermolecular distances were fabricated.[18,25] Yet other studies of porous networks via coadsorption of multi-component or multi-functional adsorbates or solvent incorporation on surfaces, producing a wide variety of interesting nanostructures, can also be found in the literature.[26–31] These results offer various routes for fabricating tunable molecular networks with tailorable nanopores potentially useful in engineering molecular sensors, molecular spintronic devices, and molecular nano heterojunctions.

We report herein a new series of 2D MPNs based on the binary system of trimesic acid (TMA) and 4,4′-bis(4-pyridyl)-biphenyl (BPBP; Figure 1a). The MPNs with nanopores of different shape and size can be formed by simply controlling the coverage ratio of the two components and the substrate temperature. Six distinct pore shapes, "rectangular", triangular, tetragonal, diamond, pentagonal, and hexagonal, were observed to date. A unified structural model was developed to systematize the observed and to predict yet unobserved structures.

All experiments were performed with an Omicron scanning tunneling microscopy (STM) in ultrahigh vacuum (UHV) with a base pressure of $< 1 \times 10^{-10}$ mbar.[20] Separate Knudsen cells containing TMA and BPBP were outgassed in UHV chamber overnight at 433 and 403 K, respectively. TMA was deposited onto a reconstructed Au(111)-$(22\sqrt{3})$ substrate at a rate of 0.01 monolayer (ML) min^{-1} from the TMA cell at 423 K. Subsequent to the formation of chicken-wire structure of TMA,[20] BPBP was deposited at a rate of 0.05 ML min^{-1} from the BPBP cell at 388 K. During the deposition of the molecules, the Au substrate was kept at room temperature. At the beginning of the experiments, the surface coverage was about 0.3 ML, ending with a coverage

[*] H. Liang, W. Sun, X. Jin, H. Li, J. Li, Prof. Dr. B. K. Teo, Prof. Dr. K. Wu
BNLMS, SKLSCUSS, College of Chemistry
and Molecular Engineering
Peking University, Beijing 100871 (China)
Fax: (+86) 10-6275-4005
E-mail: kaiwu@pku.edu.cn
Prof. Dr. X. Hu
College of Chemical Engineering and Materials Science
Zhejiang University of Technology
Hangzhou, Zhejiang (China)
E-mail: xinquan@zjut.edu.cn
Prof. Dr. B. K. Teo
Department of Chemistry, University of Illinois
Chicago, IL 60607 (USA)
E-mail: boonkteo@uic.edu

[**] This work was supported by NSFC (50821061, 20827002, 20911130229, 11004244) and MOST (2007CB936202, 2009CB929403, 2011CB808702), China.

Supporting information for this article is available on the WWW under http://dx.doi.org/10.1002/anie.201101477.

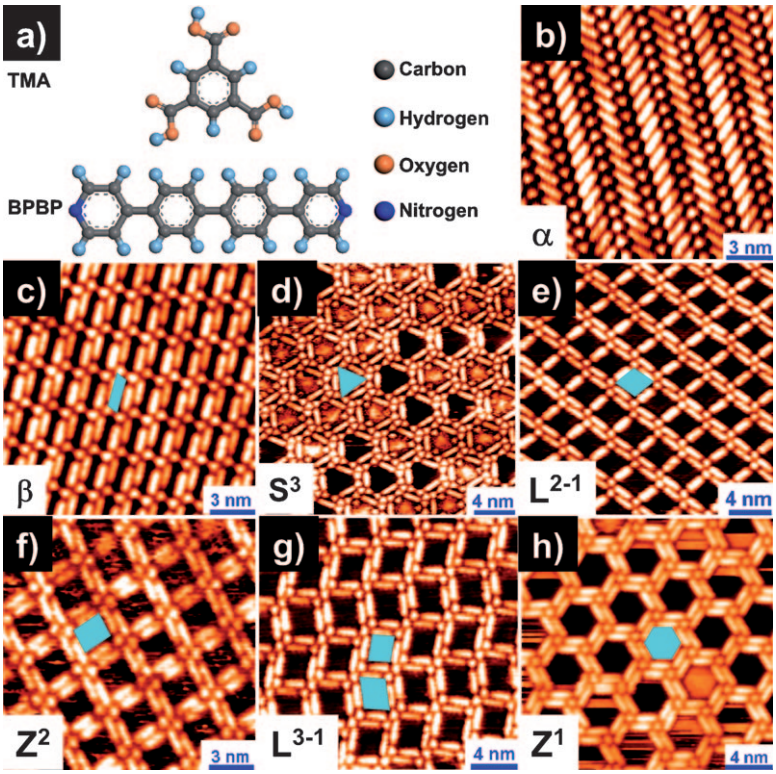

Figure 1. a) Molecular structures of TMA and BPBP. STM images of b) herringbone (α) and c) "rectangular" (β) patterns, both with TMA:BPBP ratio of 1:1. d) The S^3 pattern with TMA:BPBP ratio of 8:3; e)–h) STM images of L^{2-1}, Z^2, L^{3-1}, Z^1, with TMA:BPBP ratios of less than unity (see Figure 2). Pore sizes [nm] are: c) 0.4×2.4; d) 3.2; e) 2.0×2.3; f) 1.7×2.1; g) 1.9×2.1 and 2.0×2.5; and h) 3.1. STM scanning conditions: bias, −0.1 V; feedback current, 250 pA. The pore shapes are highlighted in blue. See text for the structural notations.

below 1.0 ML after the deposition processes. All STM images (Figure 1–3) were recorded at room temperature in constant-current mode with a tungsten tip.

Experimentally, two limiting phases, α (closed-packed herringbone structure, Figure 1b) and β ("rectangular" porous structure, pore size: $0.4\times2.4\ nm^2$, Figure 1c), both with a TMA:BPBP ratio of 1:1, were observed upon annealing above 393 K. Here the triangular and rod-like images correspond to TMA and BPBP molecules, respectively. Using the α and β phases as precursors, two experimental strategies were developed to produce various series of MPNs with TMA:BPBP ratios deviating from unity. The first strategy was to deposit increasingly more BPBP onto the substrate in a stepwise manner, giving rise to TMA:BPBP ratios of less than unity. As a result, three novel series, hereafter referred to as L^{n-m}, L^n, and Z^n, were obtained. Some examples are shown in Figure 1. Figure 2 shows a systematic enumeration of the observed nanostructures. The first series formed in this category is the L^{n-m} series, with TMA:BPBP = n:(n+1), which has a tetragonal pattern with tetragonal pores measuring (1.7–2.0) nm × (2.1–2.5) nm (see Figure 2A and examples depicted in Figure 1e and g). Further deposition of BPBPs gave rise to the L^n series, with TMA:BPBP = n:(n+1.5), which has hexagonal pores with pore sizes of approximately 3.1 nm (cf. Figure 2B). Finally, a third Z^n series was formed with TMA:BPBP = n:(n+2) which has nanopore shapes ranging from tetragonal to diamond to hexagonal (cf. Figure 2C).

The second strategy was to elevate the substrate temperature to 400 K for 1 h, causing stepwise desorption of BPBP molecules, giving rise to TMA:BPBP ratios of greater than unity. As a result, a new S^n series, with TMA:BPBP = 8:n where n = 3–6, was formed (cf. Figure 3). This series has triangular, diamond, pentagonal, and hexagonal pores for n = 3, 4, 5 and 6, respectively. The S^3 member, with a pore size of 3.2 nm, is portrayed in Figure 1d. We shall discuss each of these series in detail below.

The TMA oligomeric chains (Figure 1b and c) or clusters (Figure 1d–h) are linked by BPBPs. If we define the individual TMA oligomers or clusters as "framework knot units" (FKUs) connected by BPBPs, the MPN series can be generated by appropriate symmetry operations based on these FKU units with connecting BPBPs.

We shall first discuss the α and β phases with a TMA:BPPB ratio of unity. The TMAs in the α phase (Figure 1b) are arranged in a linear fashion and oriented in the "head-to-tail" mode. The BPBPs are oriented at approximately 60° with the TMA chain, forming a "herringbone" pattern. In contrast, the adjacent TMAs in the β phase (Figure 1c) are arranged in a zigzag fashion and oriented in the "head-to-head" mode. The BPBPs are oriented at approximately 90° with the TMA zigzag chain direction, forming "rectangular" pores.

For TMA:BPBP ratios smaller than unity, the experimentally observed FKUs (TMAs only) can be derived from either α or β phase, as enumerated in Figure 2. As depicted in Scheme 1, there are two possible orientations, α_1 and α_2, of

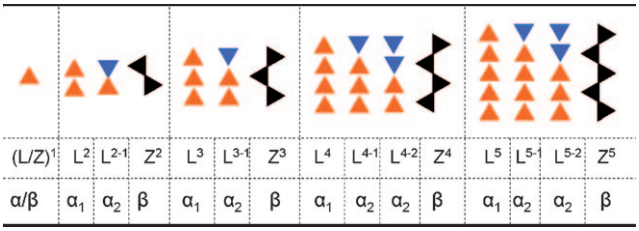

Scheme 1. All possible arrangements and orientations of the TMA molecules for the early members ($n \le 5$) of the L^{n-m}, L^n, and Z^n series.

the TMA arrangements in FKUs, derivable from the linear α phase. Herein α_1 refers to that all TMAs orient in the same direction ("head-to-tail" mode) while α_2 denotes that the TMAs orient in two opposite directions (with one, and only one, "head-to-head" connection; all others being in "head-to-tail" mode). If we use L (linear) to denote the two orientations of n TMAs in the FKUs with respect to the chain direction, then the α_1 frameworks can be represented

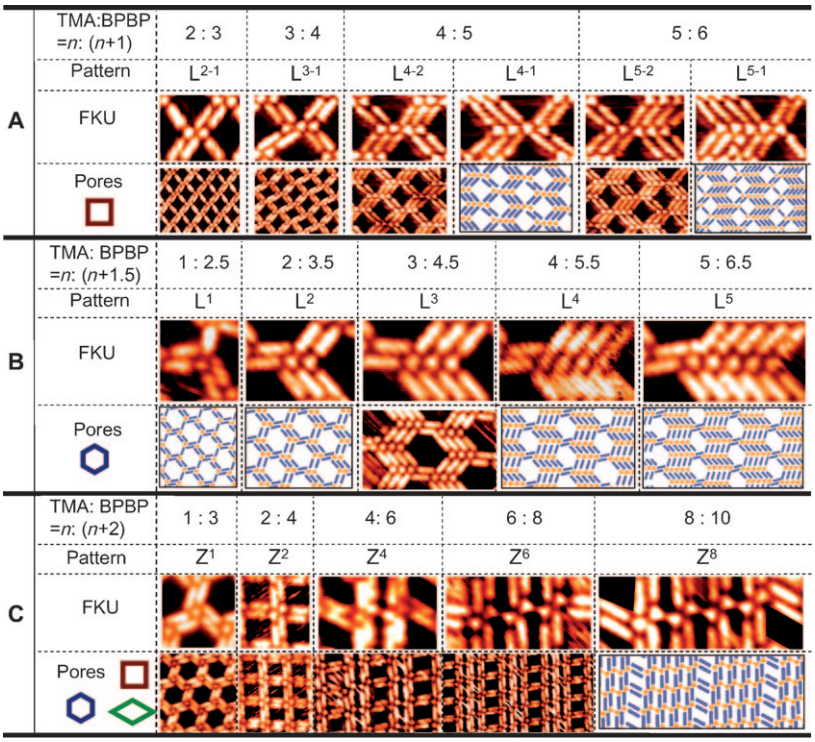

Figure 2. STM images of the observed "framework knot units" (FKUs) and the identified or predicted molecular porous networks (MPNs) series: A) the L^{n-m} series with tetragonal pores; B) the L^n series with hexagonal pores; and C) Z^n series with hexagonal, tetragonal, and diamond pores. See Supporting Information, Figure S1 for some representative large-area porous networks.

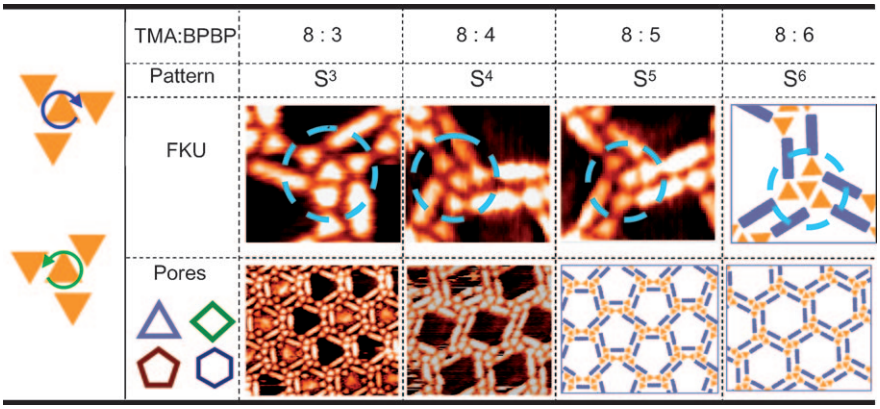

Figure 3. The "star" series, S^n, with TMA:BPBP = 8:*n*, gives rise to triangular, tetragonal/diamond, pentagonal, and hexagonal pores for $n = 3$–6, respectively. The first column depicts the TMA tetramers as the "framework knot units" (FKUs), in either clockwise or anticlockwise orientations for the three outskirting TMAs (with respect to the central one). The dashed circles indicate the observed FKUs (TMA tetramers) of the S^n series where $n = 3$–5. The missing member of the series, S^6 with hexagonal pores, is predicted; the corresponding FKU and MPN are depicted in the last column.

by L^n and the α_2 frameworks by L^{n-m} (where $m \leq n/2$, is the number of "minority" TMA molecules being oriented opposite to the $(n-m)$ ones). The zigzag arrangement of the TMAs in the FKUs (derivable from the β phase), instead, gives rise to the Z^n series where the adjacent TMAs interact exclusively in the "head-to-head" mode. All possible configurations and orientations of the FKUs for the early members ($n \leq 5$) of the three series are summarized in Scheme 1. We shall describe each of these series next.

As shown in Figure 2A, the L^{n-m} series, with TMA:BPBP = *n*:(*n*+1), gives rise to the tetragonal nanopores. The FKUs are derived from the α_2 configurations shown in Scheme 1. The L^n series, shown in Figure 2B, with TMA:BPBP = *n*:(*n*+1.5), yields instead hexagonal nanopores. The FKUs are derived from the α_1 configurations (cf. Scheme 1). Finally, the Z^n series, shown in Figure 2C, with TMA:BPBP = *n*:(*n*+2), gives rise to mixed pores: hexagonal pores for Z^1 and tetragonal or diamond pores for Z^n where *n* is an even number. The FKUs for the Z^n series are derived from the β configuration (cf. Scheme 1). A detailed examination of the Z^n series reveals that tetragonal or diamond pores of Z^n where $n = 4, 6, \ldots$ are mixed with the "rectangular" pores reminiscent of the β phase. With the exception of Z^1, odd *n* series of the Z^n configuration is unlikely to occur and thus unobserved. Z^1 is actually a member of the special case (one TMA per FKU) of the three series L^{n-m}, L^n, and Z^n with the TMA:BPBP ratio being 1:2, 1:2.5, and 1:3, respectively.

For TMA:BPBP ratios greater than unity, only one series (Figure 3) has been observed thus far. The "star" series, S^n, with TMA:BPBP = 8:*n*, where $n = 3$–6, gives rise to triangular, tetragonal, pentagonal, and hexagonal pores, respectively. Here the FKUs comprise of a "star-like" TMA tetramer, with a center TMA surrounded by three outskirting TMAs in a tail-to-tail mode.[32] The number n denotes the number of BPBPs connecting a TMA tetramer to its neighboring TMA tetramers.

In the S^3 structure, each TMA tetramer is connected to six neighboring tetramers by one TMA-TMA and one TMA-BPBP-TMA connection (Figure 3). As *n* increases, the head-to-head TMA-TMA interactions are replaced by the TMA-BPBP-TMA interactions in a stepwise manner. Eventually, only TMA-BPBP-TMA linkages are present in the predicted, yet unobserved, S^6 structure wherein each TMA tetramer is connected to only three tetramers.

The S^5 member is particularly interesting. It is well known that pentagonal structural units cannot seamlessly tile a flat 2D surface. Experimentally, we observed that the pentagonal pattern could only exist in combination with triangular or

tetragonal networks. One example is shown in Figure S2(b) in the Supporting Information.

Further scrutiny of all stable and transient porous networks of the TMA-BPBP binary system revealed that the structural patterns depended critically on the arrangements and orientations of the FKUs as well as the TMA:BPBP ratio (cf. Figures 2 and 3). Interestingly, there are three types of TMA arrangements in the FKUs: head-to-head, head-to-tail, and tail-to-tail modes, as depicted in Table 1A. Our experimental results showed that the L and Z series, with TMA:BPBP ratios of less than unity, are composed of head-to-head and head-to-tail modes, whereas the S series, with a TMA:BPBP ratio of greater than unity, comprises of tail-to-tail mode only.

Table 1: Configurations and calculated binding energies of A) three TMA-TMA interaction modes and B) four TMA-BPBP (BPBP was modeled by 4-phenylpyridine) interaction modes with hierarchical hydrogen bonds (HBs).[a]

		Head-to-Head	Head-to-Tail	Tail-to-Tail
A	HBs	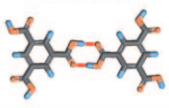	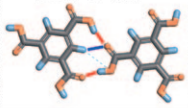	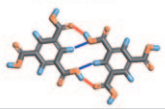
	E(eV)	-0.78	-0.41	-0.59

		T1B1	T2B1	T1B2	T2B2
B	HBs	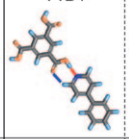	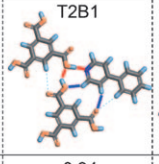	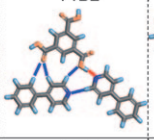	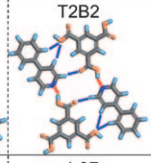
	E(eV)	-0.63	-0.94	-0.94	-1.37

[a] The red and blue lines represent strong and weak hydrogen bonds, respectively. "T" and "B" stand for TMA and BPBP, respectively.

It should be emphasized that these MPNs are made possible by the hierarchical hydrogen-bonding interactions between TMA and BPBP molecules, ranging from strong O–H···N (bonding energy, 7–8 kcal mol^{-1}) to weak C–H···O (bonding energy, 1–2 kcal mol^{-1}) hydrogen bonds.[33,34] The binding energies of the various modes of TMA-TMA and TMA-BPBP interactions are summarized in Table 1 based on our theoretical calculations described below.

We choose DFT-D[35] method to investigate inter-molecular interactions. All structures (restricted to planarity) are optimized within the RI[36]-DFT/BLYP/TZVPP level. Single point energies were calculated at the same level. For structures with more than one molecule, basis set superposition error (BSSE) corrections were included using the Counter Poise approach.[37] The package used was Turbomole[38] version 6.1. To save computation time, BPBP was modeled by 4-phenylpyridine in the calculations.

Our theoretical calculation results suggest that the weak hydrogen-bonding interactions increase with increasing proportion of BPBP molecules on the substrate; yet they have little influence on the overall stability of the porous networks. This conclusion is borne out by our experimental observation that most of the porous networks with low-index FKUs in different series have similar stabilities.

Apparently the observed MPNs represent the more stable structures, especially the low-index members of each series. Some are metastable and only observed as transient phases, e.g., the high-index members of each series. Others containing domains of two or more FKUs may be classified as hybrid patterns of the same or different series. Two such examples are depicted in the Supporting Information, illustrating the coexistence of L^2, L^3, and the α phase (Figure S2(a)) and parallel rows of S^4 and S^5 pores (Figure S2(b)). Glassy or disordered structures may also be formed, either by rapid deposition (one example is shown in Figure S3, Supporting Information) or quenching of metastable/mixed phases. These glassy or disordered structures may undergo phase transitions to form more ordered structures upon annealing at higher temperatures. Finally, more self-assembled structures can in principle exist based on the observed or yet unobserved FKUs.

In summary, the nanopores of the checkerboard motifs of the TMA-BPBP binary porous networks can be tuned by changing the surface coverage ratio of the two components and the gold substrate temperature. In particular, we succeeded in engineering the pore size and shape, from "rectangular" to triangular to tetragonal/diamond to pentagonal to hexagonal, within the binary MPNs without changing the substrate or the constituents. The observed structural patterns have been systematized and their transformation rationalized with a unified model enumerated above. The varying pore sizes and shapes make these binary MPNs potential candidates for molecular sensors, molecular devices, guest–host frameworks, spin-carrier networks, etc.

Received: February 28, 2011
Published online: June 29, 2011

Keywords: gold surface · hydrogen bonds · porous networks · scanning probe microscopy · self-assembly

[1] H. Liang, Y. He, Y. Ye, X. Xu, F. Cheng, W. Sun, X. Shao, Y. Wang, J. Li, K. Wu, *Coord. Chem. Rev.* **2009**, *253*, 2959.
[2] R. Madueno, M. T. Raisanen, C. Silien, M. Buck, *Nature* **2008**, *454*, 618.
[3] L. Bartels, *Nat. Chem.* **2010**, *2*, 87.
[4] J. A. Theobald, N. S. Oxtoby, M. A. Phillips, N. R. Champness, P. H. Beton, *Nature* **2003**, *424*, 1029.
[5] W. Xu, M. Dong, H. Gersen, E. Rauls, S. Vázquez-Campos, M. Crego-Calama, D. N. Reinhoudt, I. Stensgaard, E. Laegsgaard, T. R. Linderoth, F. Besenbacher, *Small* **2007**, *3*, 854.
[6] S. Griessl, M. Lackinger, M. Edelwirth, M. Hietschold, W. M. Heckl, *Single Mol.* **2002**, *3*, 25.
[7] N. Lin, A. Dmitriew, J. Weckesser, J. V. Barth, K. Kern, *Angew. Chem.* **2002**, *114*, 4973; *Angew. Chem. Int. Ed.* **2002**, *41*, 4779.
[8] S. L. Tait, Y. Wang, G. Costantini, N. Lin, A. Baraldi, F. Esch, L. Petaccia, S. Lizzit, K. Kern, *J. Am. Chem. Soc.* **2008**, *130*, 2108.
[9] N. Lin, A. Langner, S. L. Tait, C. Rajadurai, M. Ruben, K. Kern, *Chem. Commun.* **2007**, 4860.
[10] Z. Shi, N. Lin, *J. Am. Chem. Soc.* **2010**, *132*, 10756.
[11] F. Silly, A. Q. Shaw, M. R. Castell, G. A. D. Briggs, *Chem. Commun.* **2008**, 1907.

[12] F. Silly, A. Q. Shaw, K. Porfyrakis, J. H. Warner, A. A. R. Watt, M. R. Castell, H. Umemoto, T. Akachi, H. Shinohara, G. A. D. Briggs, *Chem. Commun.* **2008**, 4616.
[13] L. M. A. Perdigão, E. W. Perkins, J. Ma, P. A. Staniec, B. L. Rogers, N. R. Champness, P. H. Beton, *J. Phys. Chem. B* **2006**, *110*, 12539.
[14] F. Silly, U. K. Weber, A. Q. Shaw, V. M. Burlakov, M. R. Castell, G. A. D. Briggs, D. G. Pettifor, *Phys. Rev. B* **2008**, *77*, 201408.
[15] M. Treier, M. T. Nguyen, N. V. Richardson, C. Pignedoli, D. Passerone, R. Fasel, *Nano Lett.* **2009**, *9*, 126.
[16] M. A. Lingenfelder, H. Spillmann, A. Dmitriev, S. Stepanow, N. Lin, J. V. Barth, K. Kern, *Chem. Eur. J.* **2004**, *10*, 1913.
[17] A. Langner, S. L. Tait, N. Lin, C. Rajadurai, M. Ruben, K. Kern, *Proc. Natl. Acad. Sci. USA* **2007**, *104*, 17927.
[18] Y. Huang, W. Chen, H. Li, J. Ma, J. Pflaum, A. T. S. Wee, *Small* **2010**, *6*, 70.
[19] U. Schlickum, R. Decker, F. Klappenberger, G. Zoppellaro, S. Klyatskaya, M. Ruben, I. Silanes, A. Arnau, K. Kern, H. Brune, J. V. Barth, *Nano Lett.* **2007**, *7*, 3813.
[20] Y. Ye, W. Sun, Y. Wang, X. Shao, X. Xu, F. Cheng, J. Li, K. Wu, *J. Phys. Chem. C* **2007**, *111*, 10138.
[21] W. Xiao, X. Feng, P. Ruffieux, O. Gröing, K. Müllen, R. Fasel, *J. Am. Chem. Soc.* **2008**, *130*, 8910.
[22] M. Ruben, D. Payer, A. Landa, A. Comisso, C. Gattinoni, N. Lin, J.-P. Collin, J. P. Sauvage, A. De Vita, K. Kern, *J. Am. Chem. Soc.* **2006**, *128*, 15644.
[23] N. Wintjes, J. Lobo-Checa, J. Hornung, T. Samuely, F. Diederich, T. A. Jung, *J. Am. Chem. Soc.* **2010**, *132*, 7306.
[24] M. E. Cañas-Ventura, K. Aït-Mansour, P. Ruffieux, R. Rieger, K. Müllen, H. Brune, R. Fasel, *ACS Nano* **2011**, *5*, 457.
[25] X. Sun, H. T. Jonkman, F. Silly, *Nanotechnology* **2010**, *21*, 165602.
[26] J. Adisoejoso, K. Tahara, S. Okuhata, S. Lei, Y. Tobe, S. De Feyter, *Angew. Chem.* **2009**, *121*, 7489; *Angew. Chem. Int. Ed.* **2009**, *48*, 7353.
[27] F. Tao, S. L. Bernasek, *J. Am. Chem. Soc.* **2005**, *127*, 12750.
[28] S. Ahn, A. J. Matzger, *J. Am. Chem. Soc.* **2010**, *132*, 11364.
[29] S. Ahn, C. N. Morrison, A. J. Matzger, *J. Am. Chem. Soc.* **2009**, *131*, 7946.
[30] F. Tao, J. Goswami, S. L. Bernasek, *J. Phys. Chem. B* **2006**, *110*, 19562.
[31] P. Vanoppen, P. C. M. Grim, M. Rucker, S. De Feyter, G. Moessner, S. Valiyaveettil, K. Mullen, F. C. De Schryver, *J. Phys. Chem.* **1996**, *100*, 19636.
[32] We note that such a tail-to-tail mode of TMA interactions has never been observed in self-assembled systems involving TMA prior to this work.
[33] P. Vishweshwar, A. Nangia, V. M. Lynch, *J. Org. Chem.* **2002**, *67*, 556.
[34] M. Li, Y. Yang, K. Zhao, Q. Zeng, C. Wang, *J. Phys. Chem. C* **2008**, *112*, 10141.
[35] DFT-D stands for density functional theory which includes dispersion correction (see S. Grimme, *J. Comput. Chem.* **2004**, *25*, 1463 for details).
[36] M. Sierka, A. Hogekamp, R. Ahlrichs, *J. Chem. Phys.* **2003**, *118*, 9136.
[37] S. F. Boys, F. Bernardi, *Mol. Phys.* **1970**, *19*, 553.
[38] TURBOMOLE V6.1 2009, a development of University of Karlsruhe and Forschungszentrum Karlsruhe GmbH, 1989–2007, TURBOMOLE GmbH, since **2007**; available from http://www.turbomole.com.

